Biosensors and Bioelectronics 126 (2019) 806–814

Contents lists available at ScienceDirect

Biosensors and Bioelectronics

journal homepage: www.elsevier.com/locate/bios

Development of a needle shaped microelectrode for electrochemical detection of the sepsis biomarker interleukin-6 (IL-6) in real time

Christopher Russell[a], Andrew C. Ward[b], Vincent Vezza[b], Paul Hoskisson[c], David Alcorn[d], D. Paul Steenson[a], Damion K. Corrigan[b,*]

[a] School of Electronic and Electrical Engineering, University of Leeds, Leeds LS2 9JT, UK
[b] Department of Biomedical Engineering, University of Strathclyde, Glasgow G4 0NS, UK
[c] Strathclyde Institute of Pharmacy and Biomedical Science, University of Strathclyde, G4 0RE, UK
[d] Division of Anaesthesia, Royal Alexandra Hospital, Corsebar Road, Paisley PA2 9PN, UK

ARTICLE INFO

Keywords:
Electrochemical sensors
Electrochemical impedance spectroscopy (EIS)
Microelectrodes
Immunosensing
Differential pulse voltammetry

ABSTRACT

This paper outlines a simple label-free sensor system for the sensitive, real time measurement of an important protein biomarker of sepsis, using a novel microelectrode integrated onto a needle shaped substrate. Sepsis is a life threatening condition with a high mortality rate, which is characterised by dysregulation of the immune response following infection, leading to organ failure and cardiovascular collapse if untreated. Currently, sepsis testing is typically carried out by taking blood samples which are sent to a central laboratory for processing. Analysis times can be between 12 and 72 h making it notoriously difficult to diagnose and treat patients in a timely manner. The pathobiology of sepsis is becoming increasingly well understood and clinically relevant biomarkers are emerging, which could be used in conjunction with a biosensor to support real time diagnosis of sepsis. In this context, microelectrodes have the analytical advantages of reduced *iR* drop, enhanced signal to noise ratio, simplified quantification and the ability to measure in hydrodynamic situations, such as the bloodstream. In this study, arrays of eight (r = 25 μm) microelectrodes were fabricated onto needle shaped silicon substrates and electrochemically characterised in order to confirm successful sensor production and to verify whether the observed behaviour agreed with established theory. After this, the electrodes were functionalised with an antibody for interleukin-6 (IL-6) which is a protein involved in the immune response to infection and whose levels in the blood increase during progression of sepsis. The results show that IL-6 is detectable at physiologically relevant levels (pg/mL) with incubation times as short as 2.5 min. Electrochemical impedance spectroscopy (EIS) and differential pulse voltammetry (DPV) measurements were taken and DPV was concluded to be the more suitable form of measurement. In contrast to the accepted view for macro electrodes that the impedance increases upon antigen bind, we report herein a decrease in the micro electrode impedance upon binding. The small size of the fabricated devices and their needle shape make them ideal for either point of care testing or insertion into blood vessels for continuous sepsis monitoring.

1. Introduction

Sepsis is a major cause of morbidity and mortality. For example, in the United Kingdom sepsis results in the death of 37,000 individuals per year from a total of 150,000 cases and is responsible for more deaths than lung, breast and colon cancer combined (NHS England, 2015). The condition is defined as “life-threatening organ dysfunction caused by a dysregulated host response to infection”. To put this definition into perspective, even a moderate degree of organ dysfunction is associated with an in hospital mortality rate more than 10% and should a patient require admission, a mortality rate in intensive care of 30%. Full details on the consensus definition of sepsis including clinical criteria have been described recently (Singer et al., 2016). From this it is clear that improved diagnostic testing and patient management are required to enhance survival rates and patient outcomes. In current practice, there is a reliance on clinical judgment and standard laboratory techniques to diagnose sepsis, with time lags of 12–72 h for sample analysis. For example, a delay in sepsis diagnosis of one hour results in a 6–10% increase in the chance of death (Marik, 2014). It is therefore clear that the development of sensor technologies which evaluate levels of sepsis biomarkers with fast analysis times has the potential to revolutionise sepsis diagnosis and management.

* Correspondence to: Department of Biomedical Engineering, University of Strathclyde, Glasgow G1 1XQ, UK.
E-mail address: damion.corrigan@strath.ac.uk (D.K. Corrigan).

https://doi.org/10.1016/j.bios.2018.11.053
Received 14 September 2018; Received in revised form 22 November 2018; Accepted 29 November 2018
Available online 07 December 2018

A number of biomarkers have been reported in the literature as being useful for the diagnosis and monitoring of sepsis, in fact the total reported is greater than 100 (Biron et al., 2015). To develop a device capable of giving insight into the condition and its progression, it is necessary to employ a multi marker assay. In this study, we report development of a novel electrode system bearing 8 × 50 μm-diameter gold disc electrodes, which could be used as the platform for a multi marker assay, and demonstrate successful detection of a common sepsis marker.

Interleukin-6 (IL-6) is a 21 kDa glycoprotein secreted by leukocytes, which means it is defined as a cytokine: a substance which is known to be released by cells of the immune system. It is also secreted by a number of other cells, including: fibroblasts, osteoblasts, keratinocytes, endothelial cells, mesangial cells and tumour cells (Kobeissi and Zanotti-Cavazzoni, 2010). It is present at elevated levels during fever and plays an important role in the differentiation of B cells, which are antibody-producing white blood cells. IL-6 is referred to as a pro- and an anti-inflammatory cytokine because it has functions which act in both pathways. IL-6 is also an important substance for many different physiological functions, for instance bone homeostasis, due to the induction of osteoclast formation, and control of the body's metabolism. In terms of sepsis, IL-6 is a widely report as being of high importance for diagnosis and monitoring (Kibe et al., 2011; Kobeissi and Zanotti-Cavazzoni, 2010). Clinically relevant levels of IL-6 have recently been reported as being in the range of 5–25 pg/mL for physiologically normal situations and up to 1000 pg/mL in the cases of patients with sepsis (Miguel-Bayarri et al., 2012; Molano Franco et al., 2015). IL-6 and its concentration in the blood has been shown to correlate very closely with sepsis prognosis, with levels greater than 500 pg/mL leading to death in 11% of cases and greater than 7500 pg/mL leading to death in 37% of cases (Miguel-Bayarri et al., 2012; Molano Franco et al., 2015).

Microelectrode sensors have the well documented advantages of reduced *iR* drop, steady state diffusion profiles, insensitivity to convection and simplified quantification (Sosna et al., 2007). There are examples of successful fabrication of microelectrode sensors for chemical (Blair et al., 2015; Corrigan et al., 2014) and biological sensing (Corrigan et al., 2018; Quan Li et al., 2017). Herein, electrochemical impedance spectroscopy (EIS) and differential pulse voltammetery (DPV) are tested as detection strategies because both allow the non-destructive, label-free study of interfacial phenomena at electrified interfaces (Fig. 1). In EIS, by applying a small sinusoidal excitation potential and measuring the corresponding current response it is possible to probe several physical phenomena, which include: the solution resistance (R_S), the double layer capacitance (C_{DL}), the charge transfer resistance (R_{CT}) and the diffusion impedance (Warburg impedance – W) (Lisdat and Schäfer, 2008). Due to the fact that EIS is highly sensitive to changes at the electrode surface it is possible to monitor the binding of biological molecules in real time and in a label free manner (Quan Li et al., 2017). There are literature reports of effective immunosensors prepared using macroelectrodes (Ciani et al., 2012; Eissa and Zourob, 2012; Moschou et al., 2016). A common approach for the EIS based detection of protein biomarkers is to immobilise a sensing film composed of antibodies for the target analyte onto the electrode and measure alterations to R_{CT} when the target is bound. Previously developed point of care assays for IL-6 require the use of additional reagents such as sandwich assays, complex electrode preparation steps, e.g. modification with nanomaterials to improve electron transfer kinetics and optical detection techniques (Kemmler et al., 2014, 2009) or complex electrode modifications (Yang et al., 2013). In this study, we demonstrate clinically relevant levels of sensitivity without the requirement for such electrode modifications or labelling steps. Alongside EIS, DPV measurements were tested since these produce a well-defined peak current, are label-free, rapid (< 20 s), exclude non-Faradaic current contributions (due to the excitation potential waveform employed) and do not require complex interpretation such as equivalent circuit fitting (as is the case for EIS). Furthermore, the instrumentation required for DPV measurements is simple to implement at low cost. Finally, whilst many immunosensors have been successfully developed for a range of protein biomarkers using traditional electrodes, very few studies have successfully utilised true microelectrodes ($r \leq 50$ μm) for immunosensor development. The novelty of this work lies in the demonstration of a micofabricated multi-electrode array which has potential to measure important biomarkers in near real time. The system reported here simplifies electrode preparation (no need for grafting of electron transfer improving materials, e.g. graphene or nanoparticles) and has a fast time to result at clinically relevant IL-6 concentrations. Furthermore, it offers the possibility for label-free in situ monitoring for sepsis by integrating the sensor with a cannula within the bloodstream.

2. Materials and methods

2.1. Chemicals and reagents

IL-6 antibodies and antigen were purchased from Abcam (Cambridge, UK), Enterotoxin A, sulfuric acid, dithiothreitol (DTT), sulfosuccinimidyl 6-[3'-(2-pyridyldithio) propionamido] hexanoate (sulfo-LC-SPDP), potassium ferricyanide, ferrocyanide, human serum

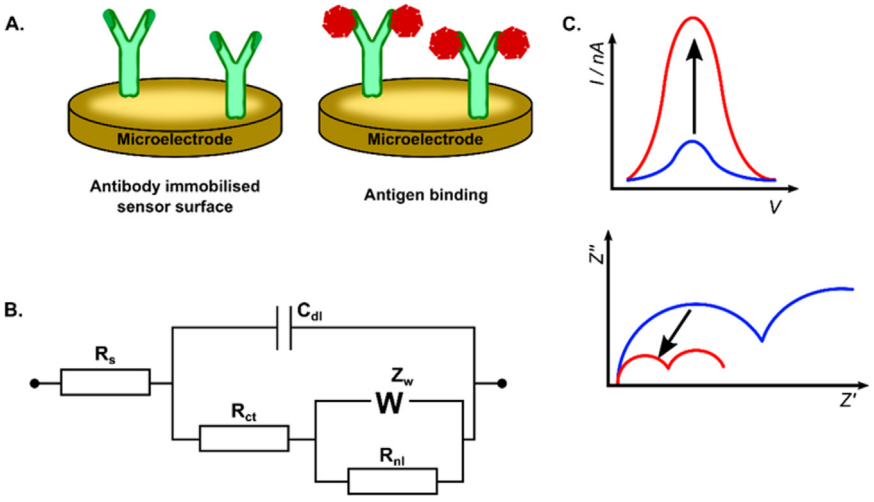

Fig. 1. (A) Electrochemical sensor principle for the antibody functionalised microelectrode including EIS and DPV measurements. (B) the modified Randles' equivalent circuit for a microelectrode. (C) EIS and DPV responses observed with the microelectrodes used in this study.

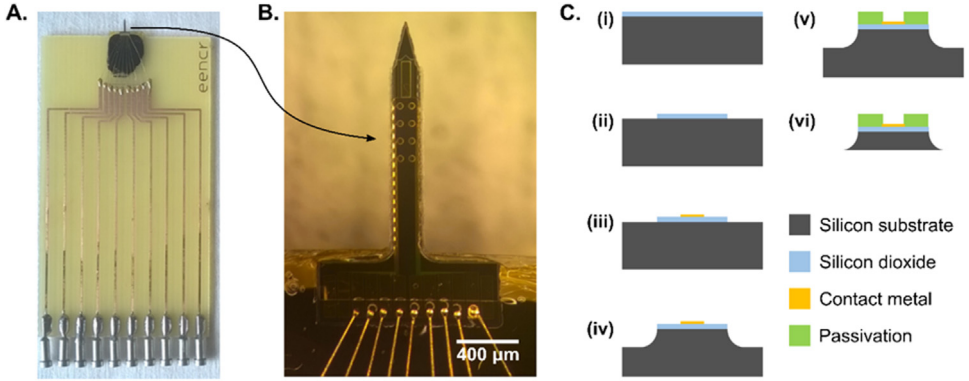

Fig. 2. (A) Image of a packaged device for electrochemical testing. (B) Image of the needle shaped electrode bearing 8 × 50 µm gold disc electrodes. (C) Outline of fabrication process employed for device production.

(sterilised) and phosphate buffered saline tablets were all purchased from Sigma Aldrich (Poole, Dorset, UK). The chemicals and reagents used for the needle electrode microfabrication are detailed in the next section.

2.2. Needle electrode microfabrication

A silicon wafer with a 1-µm-thick thermal oxide was patterned using lift-off lithography (Shipley S1830 photoresist with chlorobenzene treatment) to define a hard etch mask (100-nm-thick thermal evaporated chromium). Using reactive ion etching (15 sccm Ar / 15 sccm CHF_3; 100 W; chamber pressure 0.026 mBar), the exposed SiO_2 was etched, and the chrome mask later removed with a selective wet etch (Chromium Etchant 1020; Fig. 2.C.ii). Lift-off lithography was again used to pattern the single electrical layer comprising of interconnects and electrical contacts (8 × 50-µm-diameter disks, 1 × 300 *80 µm reference); the metal used was Ti: Au, 10:150 nm thick (Fig. 2.C.iii). A second patterned hard mask (200 nm thick thermal evaporated copper) was used for an isotropic reactive ion etch of silicon (5 sccm O_2 / 25 sccm SF_6; 100 W; chamber pressure 0.16 mBar) to define 40-µm-deep mesas (Fig. 2.C.iv). The isotropy of the etching allows the blade-like side wall of the needle to reduce dimpling and insertion force required to penetrate tissue (Hosseini et al., 2007). The copper etch mask was removed with a selective wet etch (iron nitrate solution) and a 5-µm-thick SU8 2005 (MicroChem) passivation layer was patterned protecting the electrical interconnects, and defining the area of the exposed contact (Fig. 2.C.v). The devices were protected using unexposed photoresist (S1813) and wax (Logitech quartz wax), before the reverse side of the silicon wafer was mechanically thinned using alumina grit (9 µm grit size) on a Logitech PM5 lapping and polishing machine, then polished using SF1 polishing fluid. Dissolving the wax in trichloroethylene mechanically released the silicon needles, which were later cleaned of the protective layer of photoresist in acetone (Fig. 2.C.vi). The finished 40-µm-thick needle electrodes were designed with a 240-µm-wide, 2.1-mm-long silicon tang with a taper and opening angle was 30° to further reduce the insertion force.

The electrodes were optically inspected then mounted onto a printed circuit board. Electrical interconnects were made between the gold bonding disks (LEW Technologies) on the copper tracks to the gold contacts on the needles using gold wire ball bonding (Fig. 2A–B). These wires were later passivated using varnish.

2.3. Sensor preparation and electrochemical measurements

Gold micro disc electrodes (r = 12.5 µm) were employed in order to perform benchmark cyclic voltammetry (CV), differential pulse voltammetry (DPV) and electrochemical impedance spectroscopy (EIS) measurements. Previous studies give detailed accounts of microelectrode characterisation experiments and protocols (Corrigan et al., 2018; Quan Li et al., 2017). An Autolab PGSTAT208 (Metrohm-Autolab B.V., Utrecht, Netherlands) under PC control was employed for electrochemical measurements. The reference electrode employed was a silver/silver chloride electrode in 3.0 M potassium chloride. The counter electrode was a platinum foil.

The electrode surface was functionalised by reacting equal volumes of the antibody stock solution (1 mg/mL anti Il-6 antibody, Abcam, Cambridge, UK) with 40 mM Sulfo-LC-SPDP (Sigma, Aldrich, UK) in 1 x PBS for 40 mins. The mixture was then incubated with an equal volume of 150 mM DTT (Sigma Aldrich, UK) for 1 h on a mixing plate to provide agitation. 10 µL of the solution was then drop coated onto the chip ensuring all electrodes were covered. The electrodes were stored in a humidity chamber for 16 h to allow antibody immobilisation and SAM formation to take place with the high humidity prevented evaporation of the drop. Following this, electrodes were rinsed with 1 x PBS and incubated for 1 h in 1 mM 6-mercapto-1-hexanol to backfill any unoccupied sites on the electrode surface. The electrode arrays were then left to equilibrate in 1 x PBS for 1 h prior to beginning detection of the IL-6 antigen. Further detail on the electrode functionalisation protocol can be found in a previous publication ().

EIS measurements were carried out at open circuit potential in 1 x PBS buffer containing 10 mM potassium ferricyanide and 10 mM potassium ferrocyanide. For the AC excitation signal, a total of 50 frequencies were employed ranging from 100,000–0.1 Hz (spaced logarithmically) using an amplitude of 10 mV rms. Data were fitted using the Randles' equivalent circuit and modified Randles' equivalent circuit (Fig. 1B). For some EIS responses it was necessary to fit with a modified version of the circuit (e.g. use of a resistor in parallel with the Warburg element in order to model hemispherical diffusion to a microelectrode). DPV measurements were performed using the default settings of the potentiostat instrument which were a scan rate of 0.01 Vs^{-1}, a modulation amplitude of 0.025 V, a step potential of 5 mV and a modulation time of 0.05 s.

2.4. Baseline measurements with commercial screen printed electrodes

Baseline measurements were performed using 1.6 mm Au diameter screen printed electrodes (DropSens - Au233 BT – Oviedo Spain). Electrodes were pre-treated by using an established protocol which involved holding the potential at 2 V for 120 s followed by 10 cycles between -0.25 and 1.5 V with a sweep rate of 0.1 Vs^{-1}. Once prepared the immobilisation protocol described above was employed to functionalise the surface. Impedance measurements were then carried out before and after incubation with IL-6 solutions.

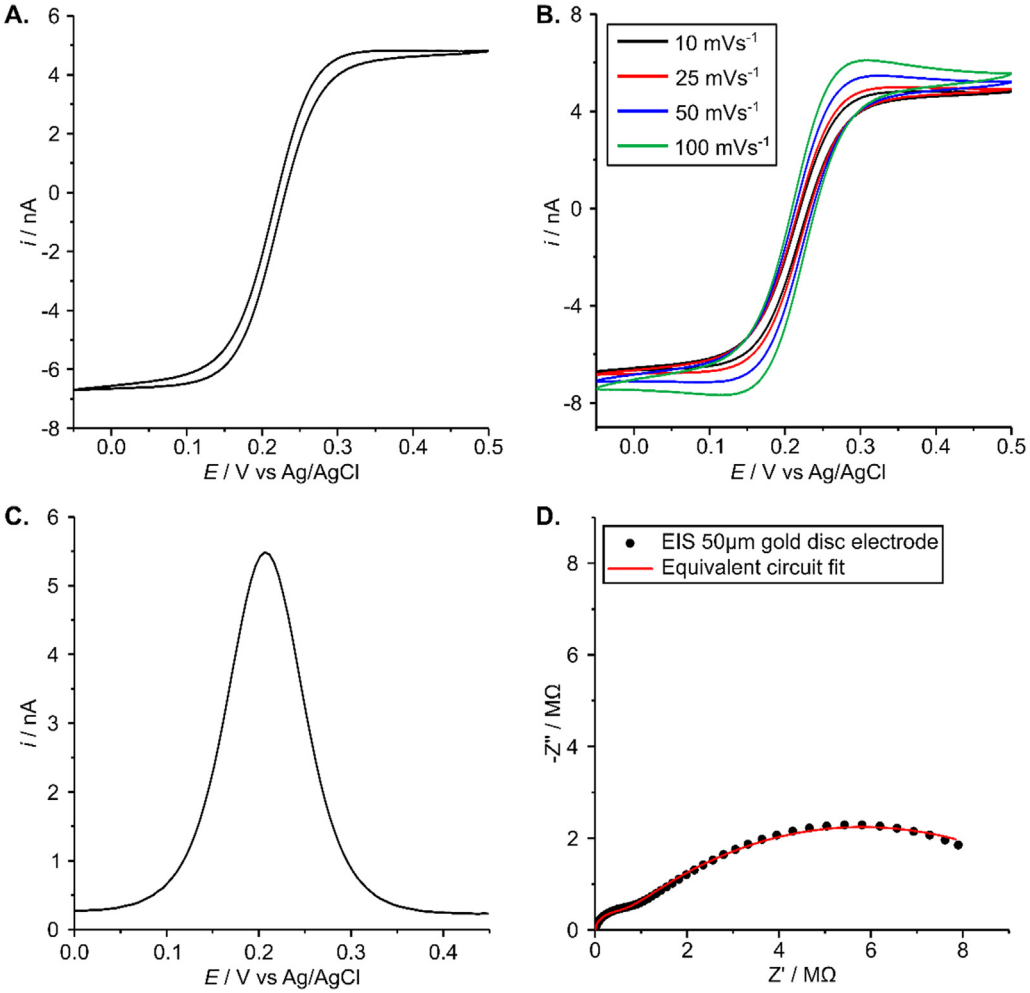

Fig. 3. Electrochemical characterisation of an $r = 25$ µm disc electrode. (A) Cyclic voltammetry (CV) at 10 mVs^{-1}. (B) Cyclic voltammetry over a range of sweep rates (10, 25, 50 and 100 mVs^{-1}). (C) Differential pulse voltammetry (DPV). (D) Electrochemical impedance spectroscopy (EIS) recorded at open circuit potential.

3. Results and discussion

3.1. Initial microelectrode characterisation

Electrodes were cleaned by cycling the voltage between -1.0 and 0.75 V for 10 cycles at a sweep rate of 100 mVs^{-1} with the maximum current limited to 100 nA in 0.1 M KCl and then transferred into a measurement buffer containing the redox agent potassium ferri-ferrocyanide and 1 × PBS as the supporting electrolyte. Cyclic voltammetry was performed using a range of scan rates along with DPV and EIS measurements to fully characterise the fabricated electrode system. It can be seen from Fig. 3 (A&B) that a sigmoidal CV response was recorded which is indicative of a microelectrode response and the development of steady state diffusion profiles during electrolysis. In addition, the CV responses showed a scan rate independence with the limiting current (I_L) values remaining broadly similar across the range of scan rates tested. There was a very slight capacitive contribution as sweep rate increased which is evident in Fig. 3B. This has been observed before with microfabricated microelectrode sensors and is attributed to parasitic capacitances (Corrigan et al., 2014). To aid with quantitation of the response the experimentally measured limiting current was compared to that calculated using the Saito equation which describes the limiting current at a microdisc electrode (Eq. (1)):

$$I_l = 4nFDcr \quad (1)$$

where I_L is the limiting current, n the number of electrons transferred, F is Faraday's constant, D is the diffusion coefficient and r the electrode radius. The experimentally determined value for I_L upon the reduction of potassium ferricyanide to ferrocyanide was found to be −6.65 nA. When the theoretical limiting current was calculated using a literature value of 7.17×10^{-6} cm^2s^{-1} for D (Konopka and McDuffie, 1970), a value of 6.9 nA was obtained. This is in good agreement with the experimentally observed current and the slight discrepancy can be explained by the recessed nature of the disc electrode (which results from the photolithographic production method) leading to a slight reduction in current compared to a flush disc where the diffusion regime is unhindered.

To further evaluate the performance of the microelectrode sensor, the EIS response was fitted using the Modified Randles' equivalent circuit for a microelectrode (see Fig. 1B) (Woodvine et al., 2010). The fitted values for R_{CT} and R_{NL} were 7.46 kΩ ± 1.19% and 10.087 MΩ ± 1.02% and the overall χ^2 'goodness of fit' was 0.004 indicating a highly satisfactory fit to the equivalent circuit. The fit can be visualised in Fig. 3D as the red line. The equations which allow estimation of these circuit parameters are outlined below

$$R_{NL} = \frac{4RT}{nFi_L} \quad (2)$$

$$R_{CT} = \frac{4RTL}{ADF^2c_\infty} \quad (3)$$

where in addition to the previous Eq. (1) L is the diffusion length and A is electrode area. Using these equations it was possible to calculate

theoretical values of 6.79 kΩ for R_{CT} and 9.01 MΩ for R_{NL}. It is important to point out that these values correspond well to the values obtained from equivalent circuit fitting and discrepancies can be accounted for by the uncertainty associated with estimating L, the slight contribution of double layer charging to the estimation of I_L and the slightly recessed nature of the electrode. These electrochemical results present a compelling case for the successful fabrication of the microelectrode array, with similar analyses previously reported in the literature to confirm successful microelectrode production using microfabrication (Corrigan et al., 2018; Terry et al., 2013).

3.2. Macro and microelectrode measurements of IL-6 binding

First of all, measurements of IL-6 binding were recorded using commercially sourced gold screen printed electrodes (SPEs) to serve as a comparison for the sensors located on the microneedle devices. These benchmark measurements were performed after first producing a SAM layer on the electrode surfaces which contained cross linked IL-6 antibodies and employed 6-mercapto-1-hexanol as a backfilling agent to prevent non-specific adsorption of analytes. This approach has been shown to produce effective immunosensing assays on gold SPE devices with detection limits for different antibody-antigen complexes in the pg/mL to fg/mL range. The measurements reported in this section were performed by testing samples of IL-6 antigen which had been prepared by spiking the protein into 1 × PBS buffer at known concentrations and then incubating at room temperature on the anti-IL-6 antibody functionalised SPE.

The results for the SPEs indicate that the overall EIS response is typical of a macroelectrode with a semi-circle for R_{CT} followed by the beginning of a 45° straight line which is representative of linear Warburg diffusion (Fig. 4A). Through equivalent circuit fitting to the established Randles' circuit (Fig. 1B), it is clear that R_{CT} increased slightly from the initial value following a ten-minute incubation of the electrode with 25 pg/mL IL-6 antigen in 1 × PBS (see SI Table S1). After establishing a baseline effect with the SPEs, equivalent measurements were performed with the microelectrode array.

The EIS response from the microelectrode sensor was evaluated pre and post incubation for 25 pg/mL IL-6 antigen and in this case it was found that the overall impedance for the electrode *decreased* following incubation with target antigen (see Fig. 4B). Both R_{CT} and R_{NL} were found to drop, indicating an increase in effective electrode area upon IL-6 binding (see SI Table S2). Interestingly, R_{CT} showed the greater percentage decrease in signal (74%) vs R_{NL} (14%) which fits with the expected response and previous data (Quan Li et al., 2017). This demonstrates that the surface area dominated R_{CT} reaction was a more sensitive measurement of receptor occupancy than R_{NL} which is a proxy for limiting current and is governed by electrodes radius rather than area (see Eqs. (2) and (3)). The finding of an increase in redox current upon IL-6 binding was also corroborated by DPV measurements which showed the peak current increased following successive incubations with IL-6 antigen. This is a surprising result since it is normally anticipated that R_{CT} increases upon exposure to target molecules in a biological binding reaction, as observed above with the commercial gold SPEs. To eliminate the possibility of experimental factors compounding the results, the tests were repeated several times alongside gold SPEs thus ruling out any defect in the antibody immobilisation or condition. In contrast to these results, it has been repeatedly reported that for macroelectrode based assays using the Faradaic impedance principle, R_{CT} increased upon successful capture of the target analyte (Corrigan et al., 2013; Ianeselli et al., 2014). Studies involving small electrodes ($r < 50$ µm) are much less common and the use of impedance as a detection technique on such small electrodes is even less frequently reported.

To determine if the unexpected drop in the impedance was unique to the needle electrodes and IL-6 combination, we undertook a series of experiments on different electrode systems. Firstly, we immobilised IL-6 onto glass pulled microelectrodes ($r = 12.5$ µm) and carried out antigen incubations following the same protocol used for the needle array. The same effect was observed and R_{CT} decreased upon incubation with target antigen. We next explored whether a decrease in R_{CT} could be observed when measurements were performed using the needle microelectrode array with DNA as the bio-receptor molecule instead of IL-6 (SI, Fig. S1). A DNA sensing film was immobilised on the electrode surface using an established protocol (Quan Li et al., 2017) and again R_{CT} was found to decrease following target binding. This suggests a common mechanism for SAM films formed on small electrode surfaces, whereby a decrease in R_{CT} and an increase in DPV peak current were indicative of target-analyte binding.

Irrespective of the direction of the impedance change, it was clear from comparing the macroelectrode response (Fig. 4A) that the sensitivity of the microelectrode to IL-6 was enhanced, with larger changes in the electrochemical signal apparent after 2.5 min incubation time, which is 75% faster than observed with the gold SPEs. Next, DPV measurements were carried out and analysed in order to provide effective comparison with the EIS based approach.

3.3. DPV measurements of IL-6 binding

Fig. 3C shows the initial DPV response of an unmodified microelectrode and Fig. 5A shows the change in DPV current from baseline with increasing IL-6 antigen concentration. These results indicate there was a decrease in DPV peak current from approximately 5.4 nA (clean electrode presented in Fig. 3C) to approximately 0.46 nA following immobilisation of the antibody layer. This is indicative of a well formed

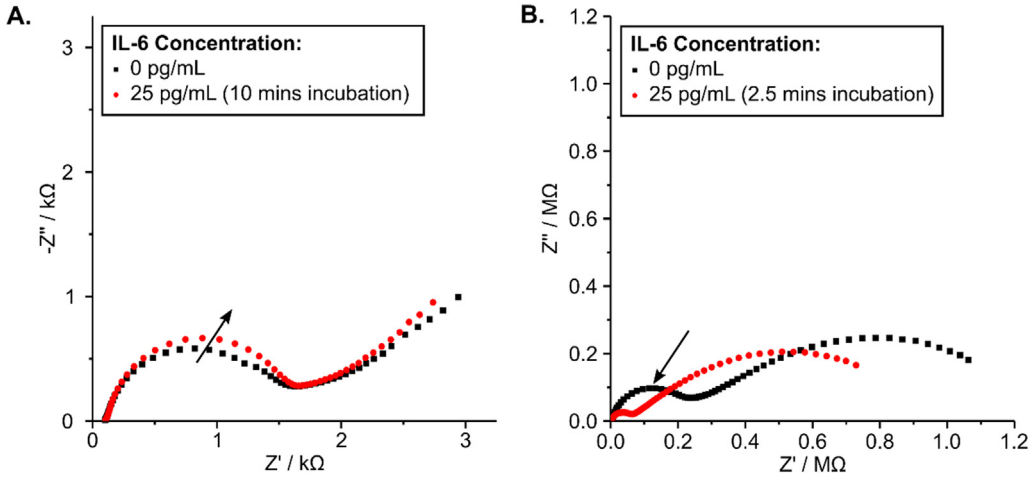

Fig. 4. Electrochemical characterisation of IL-6 antibody modified electrodes. (A) EIS response of a gold SPE macro electrode pre and post incubation (10 mins) with 25 pg/mL IL-6. (B) EIS responses from an $r = 25$ µm disc electrode pre and post incubation (2.5 mins) with 25 pg/mL IL-6. Arrows indicate direction of R_{CT} change upon IL-6 binding.

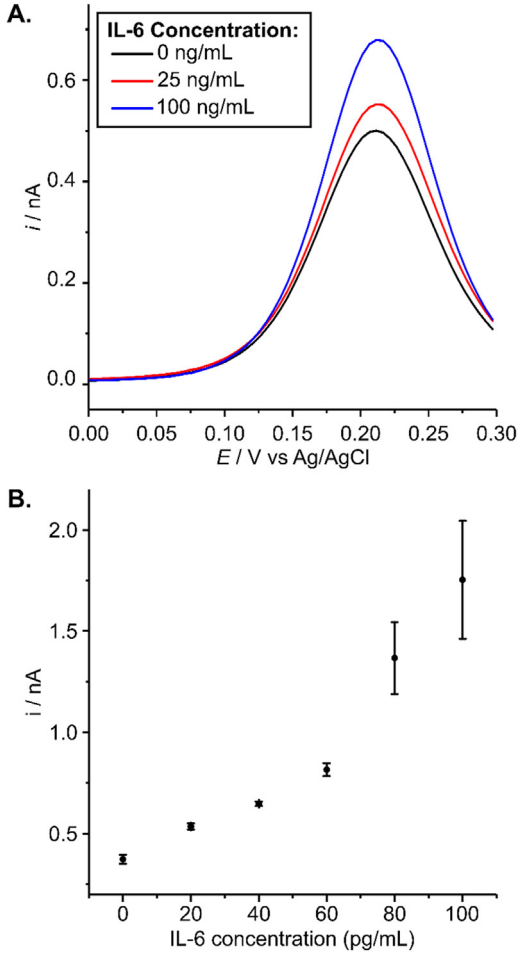

Fig. 5. (A) Example DPV peak currents following 2.5 min incubations with different concentrations of IL-6. (B) DPV peak current dose response curve recorded across a range of five IL-6 concentrations (0, 20, 40, 60, 80 and 100 pg/mL). n = 3 and bars represent S.D.

SAM which initially hampers redox agent access to the electrode surface until antigen binding increases redox agent accessibility. Furthermore, it can be seen that peak current increased with increasing IL-6 concentration following 2.5 min incubation periods. This result is consistent with the behaviour observed in the EIS measurement, i.e. R_{CT} decreased following target-antigen binding and this provides further evidence that the reported effect is an appropriate basis for sensor operation. A number of immunosensors operating on the DPV principle have been reported in the literature, showing a decrease in peak current with increasing antigen concentration (Eissa et al., 2013; Molazemhosseini et al., 2016) and is widely accepted as the normal case for macroelectrode sensors. To corroborate the findings of this study, i.e. the reverse effect, there is an example from the literature of an electrochemical sensor which also produced an increase in DPV current upon antibody-antigen binding and again involved electrodes with well-defined micro and nano features (Yi et al., 2014). The authors attribute the increase in peak current to increased surface accessibility for the redox couple following bio-recognition. Following on from the finding reported in Fig. 5A, a dose response effect was established for IL-6 modified microelectrodes (see Fig. 5B) which shows increasing DPV peak current with increasing IL-6 concentration. Between 0 and 60 pg/mL the sensor showed linear behaviour. At 80 and 100 pg/mL concentrations the current response increases in a non-linear fashion, perhaps to give a sigmoidal curve upon saturation of all binding sites. This result gives confidence in the sensor response and also shows the device is sensitive to IL-6 concentration changes in the most clinically applicable concentration range (20–100 pg/mL) which is indicative of the onset of an inflammatory response caused by sepsis. These data therefore demonstrated the suitability of DPV for measurement of antibody-antigen binding, i.e. a convenient, fast, sensitive measurement of immunocomplex formation without the requirement for labelling or complex electrode modifications.

3.4. Validation of IL-6 binding measurements and demonstration of assay sensitivity and specificity in samples simulating a biological medium

To simulate a situation more closely related to direct measurements in blood through e.g. sensor implantation, or measurement from a blood sample, the IL-6 antigen was spiked into solutions of 5% BSA (bovine serum albumin) and the sensor performance evaluated. This experiment provided the opportunity to assess the needle microelectrode array performance in the presence of potentially interfering protein species in the antigen containing incubation solution, a strategy employed in other studies (Kumar et al., 1999; Liu et al., 2013; Tomás et al., 2017). Additionally, these experiments were repeated in triplicate in order to characterise the variation inherent in both the electrodes, SAM formation and the measurement protocol. Given the consistency of behaviour between the EIS and DPV measurements, only DPV was used to assess performance in 5% BSA. First, using three electrodes from an array, sensors were incubated with IL-6 (100 pg/mL) for time intervals of 0, 2, 5, 15 and 60 mins. This concentration was selected because it represents a deviation from the normal baseline (IL-6 ~ 25 pg/mL) which is indicative of sepsis and is therefore diagnostically useful. Fig. 6A shows the resulting plot from this experiment and it can be seen that across the sixty minute time course there was a significant increase in peak current which was indicative of antigen-antibody binding. Like most immunosensors the device shows a saturation of signal which is indicative of full occupancy of all available binding sites on the sensor surface.

Demonstrating the specificity of the sensor is also a key factor in determining its performance and so to provide an example of specific vs non-specific interactions two incubation solutions were prepared. First, 250 pg/mL Enterotoxin A and second 25 pg/mL IL-6, both in 5% BSA solution. After baseline measurements, the Enterotoxin A solution was incubated on the electrode for 2.5 min and the peak current recorded, followed by a final incubation in 25 pg/mL IL-6 solution for 2.5 min. Again, this concentration was chosen because it is close to the physiologically normal concentration for IL-6 and is therefore a suitable demonstration of the ability to measure quickly at or around the clinically relevant threshold. The higher concentration of Enterotoxin A (250 pg/mL) was used to demonstrate non-specific binding with the non-specific protein ten-fold higher in concentration than the ligand. These results can be seen in Fig. 6B and provide a clear demonstration of the increase in DPV peak current resulting from the specific antibody-antigen interaction for IL-6 versus the negligible change in peak current for incubation with Enterotoxin A solution. This is the expected behaviour for an immunosensor, i.e. its operating principle is the specific interaction between antibody and antigen but this result serves as an effective demonstration of sensor specificity.

To explore the performance of the sensor in a more clinically relevant sample, short incubations were made by exposing electrodes to IL-6 spiked into human serum at a concentration of 100 pg/mL, human serum without IL-6 spiked in and phosphate buffer without IL-6 for 2.5 min (Fig. 6C). DPV measurements show a clear increase in peak current due to IL-6 binding in human serum. In contrast the serum-only incubation and the phosphate buffer control show only slight increases in peak current. This slight increase on the electrode exposed only to serum is most probably explained by non-specific protein binding slightly affecting the current. Overall, these findings give confidence that the microfabricated electrode substrates can serve as the basis of an immuno assay for IL-6 and other protein biomarkers of inflammation and sepsis.

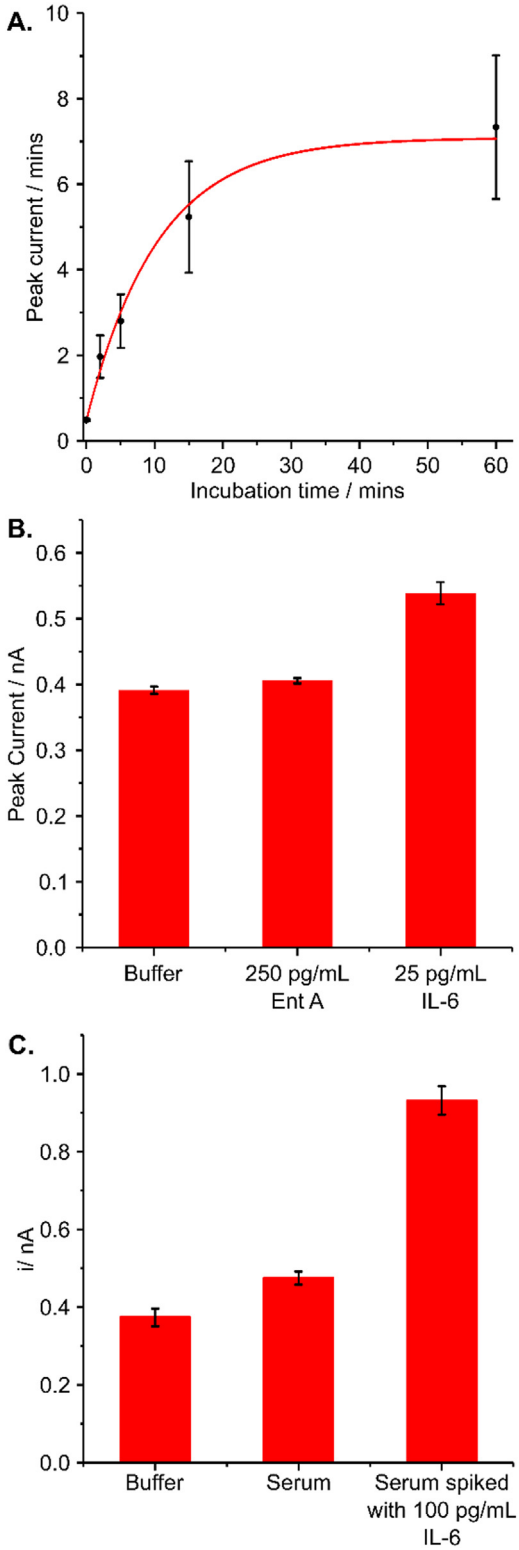

Fig. 6. (A) DPV peak current versus incubation time for microelectrodes exposed to IL-6 antigen (n = 3). (B) DPV peak current for microelectrodes incubated in buffer, with 250 pg/mL Enterotoxin A and 25 pg/mL IL-6 (n = 3) error bars in both plots represent S.D. (C) DPV peak current for microelectrodes incubated in buffer, with human serum and 100 pg/mL IL-6 spiked into human serum for 2.5 min (n = 3) error bars in all plots represent S.D.

Having fabricated, characterised and functionalised the sensor it is important to give due consideration to the observed phenomenon of a consistent decrease in R_{CT} and concomitant increase in DPV peak current upon IL-6 antigen target binding. This is most likely attributable to the formation of a densely packed SAM layer on the microelectrode sensor surface with high internal stresses and through which channels are exposed upon antigen binding allowing the redox couple better access to the electrode surface and therefore decreasing R_{CT}. There are examples in the literature of SAM forming protocols used to characterise microelectrode SAMs and which report the need for additional equivalent circuit elements to account for differences in the microelectrode response compared to the macro, for example an extra resistor can be included to model the development of well-defined pinholes which arise through use of agents such as 6-mercapto-1-hexanol (Sheffer et al., 2007) as monolayers. Here, it could be that binding of the IL-6 antigen is exposing additional pin holes in the 6-mercapto-1-hexanol layer which results in increased redox current because ferri-ferrocyanide is given better access to the electrode surface.

Similar explanations have been previously discussed in the literature for analogous effects observed on biologically modified small electrodes. Interestingly, when the χ^2 *'goodness of fits'* were analysed (SI Table S1), it can be seen that the χ^2 value for the global fit improved following target binding. Since the fit was made to the established equivalent circuit for microelectrodes, it could be inferred that IL-6 antibody-antigen binding and presentation of channels through the SAM film produced a response more typical of a microelectrode compared to the antibody functionalised electrode prior to target exposure. As previously mentioned, the effect was observed consistently when we repeated the test using glass pulled microelectrodes and also when we functionalised microfabricated microelectrode devices with single stranded probe DNA and bound a fully complementary target (SI Fig. S1).

There are also reports in the literature of R_{CT} reductions upon target binding with ferri-ferrocyanide as redox mediator when electrodes are modified with nanoscale features and are employed for detection (Manzanares-Palenzuela et al., 2016). These effects are attributed to the geometry of small electrodes opening up pores upon target hybridisation (Prasad et al., 2013), differences in the density of the sensing layer formed on micro/nanoelectrodes (Yi et al., 2014; Zhang et al., 2014) and screening of surface charges upon target binding (Jolly et al., 2015). We anticipate IL-6 carrying a net negative surface charge at the pH used to run the assay (assay pH = 7.4, isoelectric point of IL-6 ~ 6.7) (Rees et al., 1999) so believe net charge to be unlikely to account for the dose dependant decrease in R_{CT}, especially when a redox species with net negative charge such as ferri-ferro-cyanide is used as the reporter molecule. Critically, in situations where an R_{CT} decrease has been observed, experiments have been performed to show the decrease is not due to removal of the SAM layer. What is clear from this study is that the sensor displayed a consistent and dose dependant response to IL-6, in spiked buffer, in both 5% BSA and human serum, in addition the observed behaviour included typical immunosensor effects (saturation of signal upon full occupation of binding sites and high IL-6 selectivity as demonstrated by reduced sensitivity to a non-specific protein, in this case Enterotoxin A). The reported effects relating to the nature of the change in R_{CT} on the microelectrode devices are interesting and merit further investigations.

In this study, the absolute sensitivity of the device is not fully elucidated since detection focused upon the clinically relevant threshold of 20 pg/mL. Since Faradaic and non-Faradaic impedance measurements have been shown to be approximately equally sensitive this sensor can be potentially operated in both formats (Fernandes et al., 2014). When contrasting with the literature there are recent sensitivity reports for a number of biological analytes including DNA (Jin et al., 2017), dopamine (Jin et al., 2018b) and protein biomarkers (Gui et al., 2018; Jin et al., 2018a) with stated sensitivities of 0.01–1 pM (DNA), 1 nM (dopamine) and 0.3 – 500 pM (protein). With a sensitivity level of 20 pg/mL (0.95 pM) established here and using short incubation times; the sensor is competitive with current literature examples and is certainly clinically relevant.

4. Conclusions

In this work, microfabrication has allowed production of needle shaped arrays of microelectrodes. When characterised, the expected microelectrode response was observed from the sensors on the chip. Next, chemical functionalisation and assay development in buffer allowed EIS and DPV measurements of IL-6 antibody modified electrodes. This work showed that using the electrode functionalisation protocol in combination with small electrode sensors resulted in the trend of a decrease in impedance (R_{CT}) and an increase in DPV peak current following incubation with antigen samples at clinically relevant concentrations (e.g. 20 pg/mL). This effect can serve as the basis of an analytical measurement and was further tested against a non-specific protein analyte, in solutions containing BSA as a mimic of a complex sample and with IL-6 samples spiked into human serum. This sensor is an attractive candidate for further development, since beyond a SAM, it does not require any complex electrode modifications such as e.g. gold nanoparticles, graphene oxide sheets etc. and that the sensing principle was in effect label-free (the assay does not require a labelling step). Crucially the changes in the electrochemical signals were greater for the microelectrode devices than the SPEs tested and allowed detection of IL-6 concentration changes label-free and in near real time. Future work will involve development of other biomarker measurements on the chip to produce a comprehensive panel for sepsis diagnosis and improvement of the SAM layer through changes to surface functionalisation chemistry.

Acknowledgements

DC would like to thank the Dowager Countess Eleanor Peel Trust and Tenovus Scotland for seed grants in the area of sepsis monitoring. VV's EngD studentship was funded by the EPSRC CDT in Biomedical Devices and Health Technologies (EP/L015595/1). The authors are grateful for discussions with Dr Samit Chakrabarty for advice on electrode design. The underlying microelectrodes were adapted from those made for neuronal recording under the Senseback Project (EP/M025977/1) and modified for this work.

Declaration of interests

All authors have no conflicts of interest with the published study.

Appendix A. Supplementary material

Supplementary data associated with this article can be found in the online version at https://doi.org/10.1016/j.bios.2018.11.053.

References

Biron, B.M., Ayala, A., Lomas-Neira, J.L., 2015. Biomarkers for sepsis: what is and what might be? Biomark. Insights 10, 7–17. https://doi.org/10.4137/BMI.S29519.

Blair, E.O., Corrigan, D.K., Terry, J.G., Mount, A.R., Walton, A.J., 2015. Development and optimization of durable microelectrodes for quantitative electroanalysis in molten salt. J. Micro. Syst. 24, 1346–1354. https://doi.org/10.1109/JMEMS.2015.2399106.

Ciani, I., Schulze, H., Corrigan, D.K., Henihan, G., Giraud, G., Terry, J.G., Walton, A.J., Pethig, R., Ghazal, P., Crain, J., Campbell, C.J., Bachmann, T.T., Mount, A.R., 2012. Development of immunosensors for direct detection of three wound infection biomarkers at point of care using electrochemical impedance spectroscopy. Biosens. Bioelectron. 31, 413–418. https://doi.org/10.1016/j.bios.2011.11.004.

Corrigan, D.K., Blair, E.O., Terry, J.G., Walton, A.J., Mount, A.R., 2014. Enhanced electroanalysis in lithium potassium eutectic (LKE) using microfabricated square microelectrodes. Anal. Chem. 86, 11342–11348. https://doi.org/10.1021/ac5030842.

Corrigan, D.K., Schulze, H., Henihan, G., Hardie, A., Ciani, I., Giraud, G., Terry, J.G., Walton, A.J., Pethig, R., Ghazal, P., Crain, J., Campbell, C.J., Templeton, K.E., Mount, A.R., Bachmann, T.T., 2013. Development of a PCR-free electrochemical point of care test for clinical detection of methicillin resistant Staphylococcus aureus (MRSA). Analyst 138, 6997–7005. https://doi.org/10.1039/c3an01319g.

Corrigan, D.K., Vezza, V., Schulze, H., Bachmann, T.T., Mount, A.R., Walton, A.J., Terry, J.G., 2018. A microelectrode array with reproducible performance shows loss of consistency following functionalization with a self-assembled 6-mercapto-1-hexanol layer. Sens. (Switz.) 18. https://doi.org/10.3390/s18061891.

Eissa, S., L'Hocine, L., Siaj, M., Zourob, M., 2013. A graphene-based label-free voltammetric immunosensor for sensitive detection of the egg allergen ovalbumin. Analyst 138, 4378–4384. https://doi.org/10.1039/c3an36883a.

Eissa, S., Zourob, M., 2012. A graphene-based electrochemical competitive immunosensor for the sensitive detection of okadaic acid in shellfish. Nanoscale 4, 7593. https://doi.org/10.1039/c2nr32146g.

Fernandes, F.C.B., Santos, A., Martins, D.C., Góes, M.S., Bueno, P.R., 2014. Comparing label free electrochemical impedimetric and capacitive biosensing architectures. Biosens. Bioelectron. 57, 96–102. https://doi.org/10.1016/j.bios.2014.01.044.

Gui, R., Jin, H., Guo, H., Wang, Z., 2018. Recent advances and future prospects in molecularly imprinted polymers-based electrochemical biosensors. Biosens. Bioelectron. 100, 56–70. https://doi.org/10.1016/j.bios.2017.08.058.

Hosseini, N.H., Hoffmann, R., Kisban, S., Stieglitz, T., Paul, O., Ruther, P., 2007. Comparative study on the insertion behavior of cerebral microprobes. Annu. Int. Conf. IEEE Eng. Med. Biol. - Proc. 4711–4714. https://doi.org/10.1109/IEMBS.2007.4353391.

Ianeselli, L., Grenci, G., Callegari, C., Tormen, M., Casalis, L., 2014. Development of stable and reproducible biosensors based on electrochemical impedance spectroscopy: three-electrode versus two-electrode setup. Biosens. Bioelectron. 55, 1–6. https://doi.org/10.1016/j.bios.2013.11.067.

Jin, H., Gui, R., Yu, J., Lv, W., Wang, Z., 2017. Fabrication strategies, sensing modes and analytical applications of ratiometric electrochemical biosensors. Biosens. Bioelectron. 91, 523–537. https://doi.org/10.1016/j.bios.2017.01.011.

Jin, H., Guo, H., Gao, X., Gui, R., 2018a. Selective and sensitive electrochemical sensing of gastrodin based on nickel foam modified with reduced graphene oxide/silver nanoparticles complex-encapsulated molecularly imprinted polymers. Sens. Actuators, B Chem. 277, 14–21. https://doi.org/10.1016/j.snb.2018.08.156.

Jin, H., Zhao, C., Gui, R., Gao, X., Wang, Z., 2018b. Reduced graphene oxide/nile blue/gold nanoparticles complex-modified glassy carbon electrode used as a sensitive and label-free aptasensor for ratiometric electrochemical sensing of dopamine. Anal. Chim. Acta 1025, 154–162. https://doi.org/10.1016/j.aca.2018.03.036.

Jolly, P., Formisano, N., Tká˘, J., Kasák, P., Frost, C.G., Estrela, P., 2015. Sens. Actuators B: Chem. Label.-Free impedimetric aptasensor antifouling Surf. Chem.: A Prostate Specif. Antigen. case Study 209, 306–312. https://doi.org/10.1016/j.snb.2014.11.083.

Kemmler, M., Koger, B., Sulz, G., Sauer, U., Schleicher, E., Preininger, C., Brandenburg, A., 2009. Compact point-of-care system for clinical diagnostics. Sens. Actuators, B Chem. 139, 44–51. https://doi.org/10.1016/j.snb.2008.08.043.

Kemmler, M., Sauer, U., Schleicher, E., Preininger, C., Brandenburg, A., 2014. Biochip point-of-care device for sepsis diagnostics. Sens. Actuators, B Chem. 192, 205–215. https://doi.org/10.1016/j.snb.2013.10.003.

Kibe, S., Adams, K., Barlow, G., 2011. Diagnostic and prognostic biomarkers of sepsis in critical care. J. Antimicrob. Chemother. 66, 33–40. https://doi.org/10.1093/jac/dkq523.

Kobeissi, Z.A., Zanotti-Cavazzoni, S.L., 2010. Biomarkers of sepsis. Crit. Care Med. 2010, 227–228. https://doi.org/10.1016/S0734-3299(10)79402-8.

Konopka, S.J., McDuffie, B., 1970. Diffusion Coefficients of Ferri- and Ferrocyanide Ions in Aqueous Media, Using Twin-Electrode Thin-Layer Electrochemistry. Anal. Chem. 42, 1741–1746. https://doi.org/10.1021/ac50160a042.

Kumar, A.M., Fernandez, J.B., Schneiderman, N., Goodkin, K., Eisdorfer, C., Kumar, M., 1999. Simultaneous determination of 5-hydroxytryptamine, 5-hydroxytryptophan, 5-hydroxyindoleacetic acid, dopamine, and homovanillic acid in whole blood, using isocratic HPLC with electrochemical detection. J. Liq. Chromatogr. Relat. Technol. 22, 2211–2223. https://doi.org/10.1081/JLC-100101796.

Lisdat, F., Schäfer, D., 2008. The use of electrochemical impedance spectroscopy for biosensing. Anal. Bioanal. Chem. 391, 1555–1567. https://doi.org/10.1007/s00216-008-1970-7.

Liu, Y., Wang, H., Chen, J., Liu, C., Li, W., Kong, J., Yang, P., Liu, B., 2013. A sensitive microchip-based immunosensor for electrochemical detection of low-level biomarker s100b. Electroanalysis 25, 1050–1055. https://doi.org/10.1002/elan.201200525.

Manzanares-Palenzuela, C.L., Fernandes, E.G.R., Lobo-Castañón, M.J., López-Ruiz, B., Zucolotto, V., 2016. Impedance sensing of DNA hybridization onto nanostructured phthalocyanine-modified electrodes. Electrochim. Acta 221, 86–95. https://doi.org/10.1016/j.electacta.2016.10.140.

Marik, P.E., 2014. Don't miss the diagnosis of sepsis!. Crit. Care 18, 529–531. https://doi.org/10.1186/s13054-014-0529-6.

Miguel-Bayarri, V., Casanoves-Laparra, E.B., Pallás-Beneyto, L., Sancho-Chinesta, S., Martín-Osorio, L.F., Tormo-Calandín, C., Bautista-Rentero, D., 2012. Prognostic value of the biomarkers procalcitonin, interleukin-6 and C-reactive protein in severe sepsis. Med. Intensiv. 36, 556–562. https://doi.org/10.1016/j.medin.2012.01.014.

Molano Franco, D., Arevalo-Rodriguez, I., Roqué i Figuls, M., Zamora, J., 2015. Interleukin-6 for diagnosis of sepsis in critically ill adult patients. Cochrane Database Syst. Rev. https://doi.org/10.1002/14651858.CD011811.

Molazemhosseini, A., Magagnin, L., Vena, P., Liu, C.C., 2016. Single-use disposable electrochemical label-free immunosensor for detection of glycated hemoglobin (HbA1c) using differential pulse voltammetry (DPV). Sens. (Switz.) 16, 1–11. https://doi.org/10.3390/s16071024.

Moschou, D., Greathead, L., Pantelidis, P., Kelleher, P., Morgan, H., Prodromakis, T., 2016. Amperometric IFN-gamma immunosensors with commercially fabricated PCB sensing electrodes. Biosens. Bioelectron. 86, 805–810. https://doi.org/10.1016/j.bios.2016.07.075.

NHS England, 2015. Improving outcomes for patients with sepsis A cross-system action plan 9–10.

Prasad, S., Selvam, A.P., Reddy, R.K., Love, A., 2013. Silicon nanosensor for diagnosis of Cardiovascular proteomic markers. J. Lab. Autom. 18, 143–151. https://doi.org/10.1177/2211068212460038.

Quan Li, P., Piper, A., Schmueser, I., Mount, A.R., Corrigan, D.K., 2017. Impedimetric measurement of DNA-DNA hybridisation using microelectrodes with different radii for detection of methicillin resistant: Staphylococcus aureus (MRSA). Analyst 142. https://doi.org/10.1039/c7an00436b.

Rees, G.S., Ball, C., Ward, H.L., Gee, C.K., Tarrant, G., Mistry, Y., Poole, S., Bristow, A.F., 1999. Rat Interleukin 6: expression in Recombinantescherichia Coli, Purification and Development of a Novel Elisa. Cytokine 11, 95–103. https://doi.org/10.1006/cyto.1998.0408.

Sheffer, M., Vivier, V., Mandler, D., 2007. Self-assembled monolayers on Au microelectrodes. Electrochem Comm. 9, 2827–2832. https://doi.org/10.1016/j.elecom.2007.10.008.

Singer, M., Deutschman, C.S., Seymour, C.W., Shankar-Hari, M., Annane, D., Bauer, M., Angus, D.C., 2016. The Third International Consensus Definitions for Sepsis and Septic Shock (Sepsis-3). JAMA 315 (8), 801–810. https://doi.org/10.1001/jama.2016.0287.

Sosna, M., Denuault, G., Pascal, R.W., Prien, R.D., Mowlem, M., 2007. Development of a reliable microelectrode dissolved oxygen sensor. Sens. Actuators, B Chem. 123, 344–351. https://doi.org/10.1016/j.snb.2006.08.033.

Terry, J.G., Schmüser, I., Underwood, I., Corrigan, D.K., Freeman, N.J., Bunting, A.S., Mount, A.R., Walton, A.J., 2013. Nanoscale electrode arrays produced with microscale lithographic techniques for use in biomedical sensing applications. IET Nanobiotechnol. 7, 125–134. https://doi.org/10.1049/iet-nbt.2013.0049.

Tomás, R., Bristow, T., Macpherson, J., 2017. Electrochemical sensing directly in bodily fluids – a move towards point of care and in vivo analysis. Ph.D. Thesis. University of Warwick.

Woodvine, H.L., Terry, J.G., Walton, A.J., Mount, A.R., 2010. The development and characterisation of square microfabricated electrode systems. Analyst 135, 1058–1065. https://doi.org/10.1039/b924342a.

Yang, T., Wang, S., Jin, H., Bao, W., Huang, S., Wang, J., 2013. An electrochemical impedance sensor for the label-free ultrasensitive detection of interleukin-6 antigen. Sens. Actuators, B Chem. 178, 310–315. https://doi.org/10.1016/j.snb.2012.12.107.

Yi, Q., Liu, Q., Gao, F., Chen, Q., Wang, G., 2014. Application of an electrochemical immunosensor with a MWCNT/PDAA modified electrode for detection of serum trypsin. Sens. (Switz.) 14, 10203–10212. https://doi.org/10.3390/s140610203.

Zhang, W., Patel, K., Schexnider, A., Banu, S., Radadia, A.D., 2014. Nanostructuring of biosensing electrodes with nanodiamonds for antibody immobilization. ACS Nano 8, 1419–1428. https://doi.org/10.1021/nn405240g.